

Simulation of electrowetting lens and prism arrays for wavefront compensation

Juliet T. Gopinath,^{1,*} Victor M. Bright,² Carol C. Cogswell,¹ Robert D. Niederriter,³ Alexander Watson,² Ramzi Zahreddine,¹ and Robert H. Cormack¹

¹Department of Electrical, Computer, and Energy Engineering, University of Colorado, Boulder, Colorado 80309, USA

²Department of Mechanical Engineering, University of Colorado, Boulder, Colorado 80309, USA

³Department of Physics, University of Colorado, Boulder, Colorado 80309, USA

*Corresponding author: julietg@colorado.edu

Received 14 June 2012; revised 20 August 2012; accepted 20 August 2012;
posted 20 August 2012 (Doc. ID 170158); published 18 September 2012

A novel application of electrowetting devices has been simulated: wavefront correction using an array of electrowetting lenses and prisms. Five waves of distortion can be corrected with Strehl ratios of 0.9 or higher, utilizing piston, tip-tilt, and curvature corrections from arrays of 19 elements and fill factors as low as 40%. Effective control of piston can be achieved by placing the liquid lens array at the focus of two microlens arrays. Seven waves of piston delay can be generated with variation in focal length between 1.5 and 500 mm. © 2012 Optical Society of America

OCIS codes: 010.1080, 230.0230, 010.1285.

1. Introduction

Optical free-space communications and tracking are important tools for both the civilian and defense sectors. While optical free-space links are versatile and can be easily erected (unlike fiber optic links), they suffer from atmospheric and oceanic distortion caused by index variations [1]. This distortion destroys valuable information and degrades the signal-to-noise ratio of the optical link. Tunable optofluidic lens and prism arrays can be used to both measure and correct the wavefront distortion in a more versatile manner than existing adaptive optics approaches [2]. In contrast to other solutions, the lens and prism arrays operate in transmission, simplifying implementation in optical systems. The lens and prism arrays have the capability to compensate wavefront curvature, tip-tilt, and piston, using micrometer- to millimeter-scale elements with lower voltages than competing adaptive optic technology. These

properties allow the technology to be inserted into cameras and other compact electronics. The goal of this work is to demonstrate the suitability of electrowetting lens and prism arrays for wavefront correction.

The simulated tunable lens and prism arrays described here are based on electrowetting [3], in which the forces from an applied voltage shape a droplet of liquid, as shown in Fig. 1. The contact angles of a small liquid droplet on an insulated metallic substrate will be determined by the balance in surface tension at each interface: substrate/liquid, substrate/surrounding medium, and liquid/surrounding medium. Young's equation can be used to determine the contact angle of a droplet with a solid, planar substrate [1,2]:

$$\gamma_{LG} \cos \theta = \gamma_{SG} - \gamma_{SL},$$

where γ is the surface tension between the two media, S represents the substrate, L represents the liquid, G represents the surrounding medium, and θ is the contact angle of the droplet with the substrate.

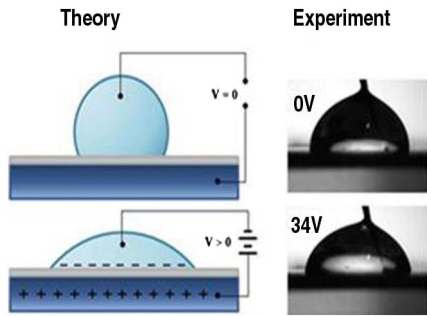


Fig. 1. (Color online) Concept of electrowetting. Applying a voltage to a conducting liquid changes the contact angle between the liquid and the conductive layer beneath. If the liquid is instead placed in a cylindrical (or tapered) chamber with contacts on both sides, an applied voltage changes the contact angle of the liquid to the side walls, producing a variable focus lens. (Left) Theory. (Right) Experiments performed using a droplet of deionized water mixed with 1% sodium dodecyl sulfate placed on Teflon. Two different voltages were applied, 0 V and 34 V, and show the broadening and flattening of the droplet with increasing voltage as predicted by theory. Note a portion of the voltage wire is shown protruding from the top of the droplet.

The effect of an applied voltage to the liquid and the substrate on the contact angle of the droplet is given by

$$\gamma = \gamma_o - \frac{1}{2}cV^2,$$

where γ_o is the surface tension without an applied voltage and c is the capacitance per unit area in the interface. This expression can be modified for the case of a droplet on a dielectric, rather than metal, surface:

$$\gamma_{SL} = \gamma_o - \frac{1}{2} \frac{\epsilon\epsilon_o}{d} V^2,$$

where ϵ is the relative permittivity of the dielectric layer, ϵ_o is the permittivity of vacuum, d is the thickness of the dielectric layer, and V is the voltage across the dielectric layer. The expression for the contact angle is given by the Lippmann–Young equation:

$$\cos \theta = \cos \theta_o + \frac{\epsilon\epsilon_o}{2\gamma_{LG}d} V^2,$$

where θ_o is the contact angle of the droplet with no applied voltage. The contact angle sensitivity to voltage can be enhanced with the insertion of a hydrophobic layer between a conducting liquid and the electrode and with a thinner dielectric layer. For lenses, the liquid is generally placed on a set of electrodes or in a cylindrical aperture with contacts on the interior wall and bottom or top. An applied voltage determines the contact angle of the liquid to the side wall, allowing variable lens focus. To apply voltage to arrays of lenses and prisms, one electrode needs to be incorporated in the sidewall of the lens or prism. The other electrode can be patterned on a substrate that is in contact with the conductive

liquid. A schematic of a typical lens is shown in Fig. 2(a). Similarly, in Fig. 2(b), a square aperture design with contacts on opposing sides produces a prism shape that yields variable deflection angles when differing voltages are applied to the two sides.

Electrowetting devices are particularly attractive for adaptive optical applications due to their size, robustness, fast response time, low insertion loss, polarization insensitivity, and lack of bulky peripherals [4–6]. These favorable properties make them a more versatile solution than technologies such as spatial light modulators [7,8], microelectromechanical segmented (MEMS) and deformable mirror systems [9–12], piezo-actuated deformable mirrors [13], and flexible membrane liquid lenses [14–16].

Key differences between electrowetting technology and other adaptive optic approaches are summarized in Table 1. Electrowetting devices can operate at kilohertz speeds, with gigahertz speeds being demonstrated recently in a carbon nanotube device [17] compared with kilohertz for MEMS devices. The switching speed is proportional to $\sqrt{\frac{\rho v}{\gamma}}$, where ρ is density, v is volume, and γ is surface tension. Electrowetting lenses and prisms have been shown with dimensions down to 300 μm , which compares well with tens of micrometers for MEMS devices. They have also been shown to operate over diopter ranges from –100 to 50 [5] and 230 to 360 [18]. MEMS continuous and segmented deformable mirrors require hundreds of volts for operation, while comparable electrowetting lenses only require tens of volts. Electrowetting lenses with focal lengths ranging from 2.3 mm to infinity have been demonstrated with 45 V [4]. Operating voltages for electrowetting lenses can be further reduced by using a surfactant to reduce surface tension [19]. Alternatively, electrowetting based on the interface between two immiscible electrolytic solutions rather than dielectric has been demonstrated to yield contact angle changes of over 40 deg for operation under 1 V [20]. Another competing technology is the spatial light modulator (SLM). However, in contrast to electrowetting devices, liquid-crystal-based SLMs are polarization sensitive and operate at hertz speeds. SLMs can compensate piston, but not curvature, unlike electrowetting lenses, which can do both. Pressure-driven liquid lenses are another alternative. Fabrication of

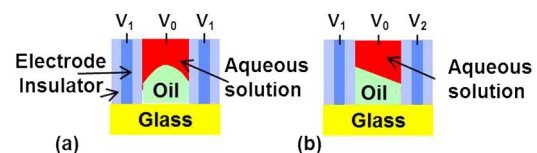


Fig. 2. (Color online) (a) Electrowetting lens schematic. The liquid is placed in a cylindrical aperture with contacts on the interior wall and top. An applied voltage determines the contact angle of the liquid to the side wall, allowing variable lens focus. (b) Electrowetting prism schematic. A square aperture design with contacts on opposing sides produces a prism shape that yields variable deflection angles when differing voltages are applied to the two sides.

Table 1. Comparison of Adaptive Optic Technologies

Adaptive Optic Technology	Curvature Correction	Tip-Tilt Correction	Piston Correction	Speed	Size	Pol. ^a Insensitive	Transmission	Voltage Required (V)
Deformable mirror	Y	Y	Y	kHz	mm-cm	Y	N	100 s
MEMS segmented micromirror	N	Y	Y	kHz	μm	Y	N	100 s
Spatial light modulator	N	N	Y	Hz	μm-mm	N	Y	10 s
Pressure-driven liquid lenses	Y	N	Y	Hz	mm-cm	Y	Y	10 s
Electrowetting lens and prism arrays	Y	Y	Y	kHz	μm-mm	Y	Y	10 s

^aPol., polarization.

pressure-driven lenses is complex for small diameters, and the response speed is slow. Additionally, because a flexible polymer is needed to form the top curved surface, lens quality can be problematic.

Electrowetting lenses are best suited to applications requiring small, high-quality lenses. Appropriate choice of liquids will allow mitigation of gravity and temperature effects due to density mismatch as well as impacting response speed. The effect of gravity on the lenses has been simulated. At large diameters, greater than 6 mm, for a typical silicone oil and water mixture, gravity distorts the perfectly spherical surface achievable with electrowetting by only $\lambda/17$ [21,22]. At small diameters (< few millimeters), gravity has minimal effects on the spherical surfaces for liquids of similar density (oil and water), and response speeds improve with smaller volumes. Additionally, the optical quality of electrowetting lenses has been measured to be comparable to fixed microlenses [4,22].

The electrowetting lens and prism arrays can be used to provide all the necessary adjustments for a wavefront: tip-tilt, curvature, and piston. By varying the focal lengths of individual elements, the lens arrays can be used to correct wavefront curvature, while prism arrays can be used to alter the wavefront tip-tilt. The piston (optical path length) can also be controlled by changing the power of an electrowetting lens. Because the lens is formed from a constant volume of fluid with fixed side walls, its center thickness (and hence phase delay) is a function of the curvature of the end surface. Unfortunately, this effect is tied to the power of the lens. However, by placing an electrowetting lens array at the focal point of a two-lens telescope, one can adjust the piston independent of the wavefront curvature. We have simulated the wavefront correction potential of an array of electrowetting lenses and prisms and have shown that this is an effective method for compensation of atmospheric distortion and phase control. Five waves of distortion can be corrected with Strehl ratios of 0.9 or higher, utilizing piston, tip-tilt, and curvature corrections from 19-element arrays and fill factors as low as 40%. In addition, up to seven waves of piston delay can be generated with variation in focal length between 1.5 and 500 mm. We anticipate using three to four arrays for initial proof-of-concept experiments to control all four variables. In the future, we will

pursue integrated lens and prism arrays on a single chip to decrease the number of adaptive elements in the system to two. With postprocessing, a Shack-Hartmann wavefront sensor can be used to determine all four quantities that provide feedback to an adaptive optics system. Additionally, a hill climbing algorithm [23] can be used to optimize a single measurement of beam quality through adjustment in tip-tilt, curvature, and piston.

2. Method

We have simulated the effect of atmospheric distortion on our individually addressable lens and prism arrays using a Zemax software model, based on ray tracing, at a wavelength of 550 nm. For each ray traced through the system, Zemax stores the ray's path length (phase) and the point of intersection with the image plane. Each ray is considered to represent a plane wave propagating in the same direction, with the same phase along the ray path. At the image plane, the plane waves represented by each ray are added up coherently to form the point spread function (PSF).

The algorithm used to adjust tip-tilt, curvature, and piston operates by sequentially optimizing each parameter. First, curvature of each element is adjusted to achieve the smallest spot. Next, tip-tilt is adjusted to overlap all the spots on top of each other. Finally, piston is used to provide the final phase adjustments. The most important adjustment is tip-tilt, as distortion adds speckle that requires tip-tilt correction. In our model, we are only correcting the on-axis field, and vignetting is not an issue.

Figure 3(a) illustrates the setup for simulating the compensation effects of the lens and prism arrays. First, a randomly generated amount of distortion is added to the input wavefront. The light then propagates through a prism and lens array capable of tip-tilt, piston, and curvature correction, and then another lens focuses the light onto a detector, which measures the PSF and Strehl ratio. An array of 19 lenses was simulated, each formed by 2 mm diameter water droplets. Lens and prism action was achieved at the water-air interface. Tip-tilt was varied from 2.9×10^{-5} to 0.12 deg, focal lengths from infinity to -0.827 m, and piston from 0 to 4.7 waves. These parameters are realistic, based on experimental demonstrations. Electrowetting lenses have been

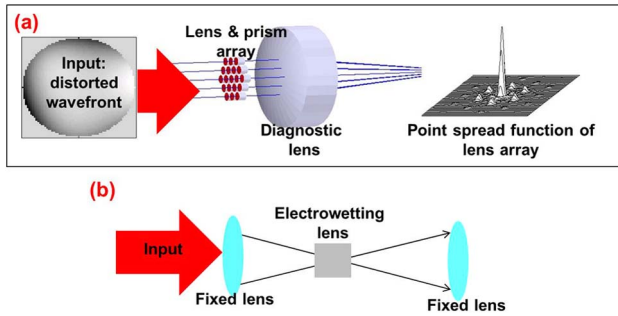


Fig. 3. (Color online) Setups for simulations. (a) A distorted wave is input to a 19-element lens and prism array. A diagnostic lens focuses the resulting corrected wavefront, and the PSF of the lens array and Strehl ratio are measured. (b) Light is input to a telescope with an electro-wetting element placed at the focus. This setup is used to evaluate the piston-adjustment capabilities of the electro-wetting lens.

demonstrated with diopter ranges between -100 to 50 [5], and prisms with steering up to 14 deg [6]. The effect of gravity on the 2 mm diameter lenslets containing a water and air interface has been modeled and found to be negligible. Gravitational effects only produce a $\lambda/50$ distortion from a spherical surface. A full model for the lenses and prisms based on experimental parameters will be developed after the prototypes are built.

We have run simulations for compensation with different fill factors. The fill factor is defined as the percentage of area occupied by the lenses compared with the necessary unused area between the lenses. We have also run simulations with piston correction omitted and for a range of visible wavelengths.

In addition to simulating distortion with random combinations of Zernike polynomials, we have also run calculations using Kolmogorov statistics. The Wiener phase spectrum [24] was used to set the amplitudes of an array that makes up the wavefront

$$\varphi(k) = \left(\frac{0.023}{r_o^{5/3}} \right) k^{-11/3},$$

where r_o is the Fried parameter and k is spatial frequency. Random phases were added to the array coefficients, and the entire array was Fourier transformed to yield a phase screen, using an aperture size of 20 mm and a central wavelength of 550 nm. The Fried parameter is defined to be the diameter over which there is 1 radian of phase variation in the wavefront.

The effect of piston delay achievable with the lenses was simulated using the setup in Fig. 3(b). For these simulations, the lens is filled with water and oil, and lensing occurs at the interface between the water and oil. Similar results would be obtained using a water and air interface. An electro-wetting lens array is placed at the focal point between two microlens arrays. By adjusting the focus of the electro-wetting lenses, the piston delay is varied. The light is focused through the center of the lenses and experiences a path length change when the

curvature (focal length) of the lens is varied. Thus, by combining all of the described techniques into one optical system, we can simultaneously correct wavefront curvature, tip-tilt, and piston using only electro-wetting lens and prism arrays.

3. Results

Figure 4 shows the results of distortion compensation as a function of input distortion and fill factor for a 19-element lens array, with elements that are 2 mm in diameter, 2 mm in thickness, and filled with water. Output Strehl ratio is plotted versus input distortion in waves for a variety of different fill factors: 40% , 58% , and 80% . The simulation includes a combination of tip-tilt, curvature, and piston compensation.

The input distortions were generated with a random wavefront generated from Zernike polynomials. Maximum peak to valley differences were used to calculate the total distortion. The random nature of the generated distortions leads to some noise on the plots. For input distortions up to 5 waves, the plots show that it is possible to generate Strehl ratios above 0.9 with control of piston, tip-tilt, and curvature, even with only 40% fill factor. Current technology easily permits fabrication of lenses with 40% – 60% fill factors, and with modifications, it may be possible to achieve 80% fill factors. To improve compensation for larger distortions, higher fill factor arrays need to be used.

To investigate chromatic effects, simulations were run for wavelengths of 486 , 587 , and 656 nm to model the corrective power of the devices, taking into account the dispersion of the water-based liquid lenses. Correction was still achieved, but with lower overall Strehl ratios. For two waves of distortion, we were able to improve the Strehl ratio of the system from 0.290 to 0.443 in contrast to the single wavelength case where the Strehl ratio was improved from 0.516 to 0.973 . Careful choice of liquids will allow chromatic effects in electro-wetting lenses to be

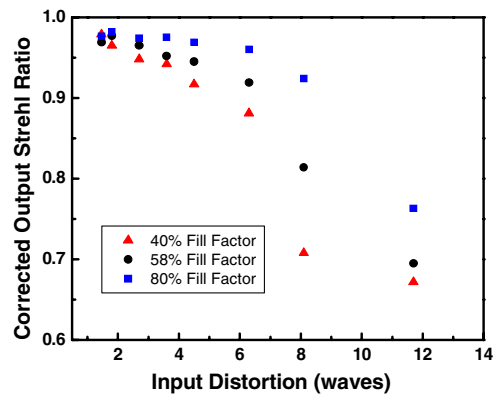


Fig. 4. (Color online) Output Strehl ratio versus input distortion in waves for a variety of different fill factors for a lens and prism array: 40% fill factor (red triangles), 58% fill factor (black circles), and 80% fill factor (blue squares). Simulation includes tip-tilt, curvature, and piston compensation. The arrays consist of 19 elements that are 2 mm in diameter and are filled with water and air.

mitigated. Figure 5 plots the output Strehl ratio versus the ratio of the lens center-to-center spacing to the Fried parameter. The simulations were performed using Kolmogorov statistics, and each point is averaged over three datasets. The green squares represent tip-tilt, curvature, and piston correction, while the black triangles represent only tip-tilt and curvature correction. The simulations were run for an array of 19 2 mm diameter lenses that are filled with water and air and arranged with a 58% fill factor. The results without piston correction still demonstrate a substantial amount of correction. Other cases using curvature/piston correction, tip-tilt/piston correction, or piston correction alone do not display improvement in Strehl ratio with correction. Our algorithm requires piston and tip-tilt correction in order to achieve reasonable quality of output spots. The main correction from distortion is due to speckle, which is most affected by adjustments in tip-tilt and curvature.

Figure 6 explores the amount of piston achievable for a given focal length. The simulation is run for lenses 1 mm in diameter that are filled with a mixture of water and oil. Seven waves of delay can be produced by changing the focal length from 1.5 to 500 mm, and even a small change in focal length of 1.5 to 2.5 mm can produce 3 waves of delay. As the lens curvature becomes flatter (corresponding to longer focal length), larger changes in focal length are needed to produce piston delay. Since current electrowetting lenses [4] have been demonstrated with focal length ranges between 2.8 to 20 mm, these results demonstrate that many waves of piston delay are possible. Lens arrays in this configuration can be used in many applications. One example is as a phase modulator to coherently combine arrays of fibers or diode lasers. The response time of the lenses is set by the size and type of liquids that are used to generate the lensing effect. Current response times

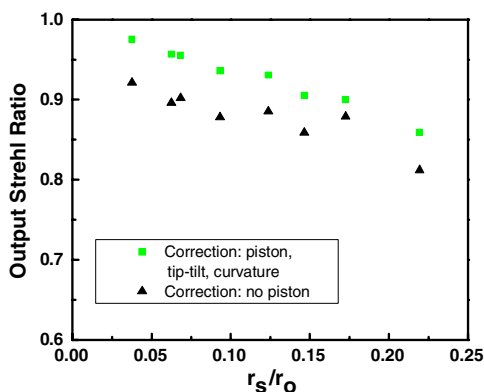


Fig. 5. (Color online) Simulations of output Strehl ratio achievable versus r_s/r_o , the ratio of lens center spacing to the Fried parameter. The simulations were performed using Kolmogorov statistics, and each point is averaged. The green squares represent tip-tilt, curvature, and piston correction while the black triangles represent tip-tilt and curvature correction. The simulations were run for an array of 19 2 mm diameter lenses that are filled with water and air and arranged with a 58% fill factor.

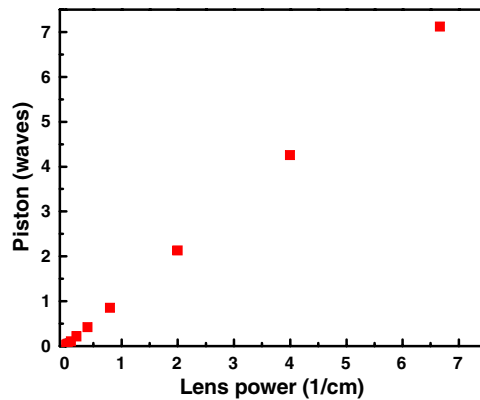


Fig. 6. (Color online) Effect of focal length tuning on piston compensation for 1 mm diameter lenses with 2 mm thickness containing equal quantities of oil and water. As the lens curvature becomes flatter (corresponding to longer focal length), larger changes in focal length are needed to produce piston delay.

from millimeter-size lenses are of the order of milliseconds, so kilohertz feedback to stabilize phases between elements is possible.

4. Conclusions

We have shown that electrowetting lens and prism technology can be used for wavefront correction, providing curvature, tip-tilt, and piston control. Large amounts of distortion can be corrected using combinations of all three controls, including a significant amount of piston delay, which can be generated for small changes in focal length. Significant improvements are possible without piston correction as illustrated in Fig. 5. Given the parameters of the devices, tip-tilt and curvature correction is needed. The parameters used in the simulation reflect realistic parameters for actual devices. The technology has the potential for a wide range of applications, ranging from atmospheric and oceanic distortion compensation for imaging and tracking systems to coherent beam combining and microscopy. The amount of distortion compensation possible shows that electrowetting microlenses and prism arrays are a promising adaptive optics technology. The large amount of piston control available opens the possibility of applications in coherent beam combining or arbitrary waveform generation with fiber or diode laser arrays. In the future, we will pursue wavefront correction with electrowetting lens and prism arrays experimentally.

This work is sponsored by the 2011 Office of Naval Research CNR Challenge Program, Award N00014-11-1-0574. We acknowledge technical discussions with Dr. Keith Cobry. Robert Niederriter was supported by the Department of Defense (DoD) through the National Defense Science & Engineering Graduate (NDSEG) Fellowship Program.

References

1. N. S. Kopeika, "A System Engineering Approach to Imaging," (SPIE, 1998).
2. R. K. Tyson, "Principles of Adaptive Optics," (CRC Press, 2011).

3. F. Mugele and J.-C. Baret, "Electrowetting: from basics to applications," *J. Phys. Condens. Matt.* **17**, R705–R774 (2005).
4. F. Krogmann, W. Moench, and H. Zappe, "A MEMS-based variable micro-lens system," *J. Opt. A* **8**, S330–S336 (2006).
5. S. Kuiper and B. H. W. Hendriks, "Variable-focus liquid lens for miniature cameras," *Appl. Phys. Lett.* **85**, 1128–1130 (2004).
6. W. Han, J. W. Haus, P. McManamon, J. Heikenfeld, N. Smith, and J. Yang, "Transmissive beam steering through electrowetting micropism arrays," *Opt. Commun.* **283**, 1174–1181 (2010).
7. G. D. Love, "Wave-front correction and production of Zernike modes with a liquid-crystal spatial light modulator," *Appl. Opt.* **36**, 1517–1524 (1997).
8. C. Warde, A. D. Fisher, D. M. Cocco, and M. Y. Burmawi, "Microchannel spatial light modulator," *Opt. Lett.* **3**, 196–198 (1978).
9. T. Weyrauch, M. A. Vorontsov, T. G. Bifano, A. Tuantranont, V. M. Bright, J. Karpinsky, and J. Hammer, "Performance evaluation of micromachined mirror arrays for adaptive optics," *Proc. SPIE* **4124**, 32–41 (2000).
10. L. Z. Schatzberg, T. Bifano, S. Cornelissen, J. Stewart, and Z. Bleier, "Secure optical communication system utilizing deformable MEMS mirrors," *Proc. SPIE* **7209**, 72090C (2009).
11. M. C. Roggemann, V. M. Bright, B. M. Welsh, W. D. Cowan, and M. Lett, "Micro-electro-mechanical deformable mirrors for aberration control in optical systems," *Opt. Quantum Electron.* **31**, 451–468 (1999).
12. W. D. Cowan, M. K. Lee, B. M. Welsh, V. M. Bright, and M. C. Roggemann, "Surface micromachined segmented mirrors for adaptive optics," *IEEE J. Sel. Top. Quantum Electron.* **5**, 90–101 (1999).
13. M. A. Ealey and J. A. Wellman, "Deformable mirrors: design fundamentals, key performance specifications, and parametric trades," *Proc. SPIE* **1543**, 36–51 (1992).
14. H. Ren, D. Fox, P. A. Anderson, B. Wu, and S.-T. Wu, "Tunable-focus liquid lens controlled using a servo motor," *Opt. Express* **14**, 8031–8036 (2006).
15. Y. Hongbin, Z. Guangya, C. F. Siong, and L. Feiwen, "Optofluidic variable aperture," *Opt. Lett.* **33**, 548–550 (2008).
16. D.-Y. Zhang, N. Justis, V. Lien, Y. Berdichevsky, and Y.-H. Lo, "High-performance fluidic adaptive lenses," *Appl. Opt.* **43**, 783–787 (2004).
17. J. Y. Chen, A. Kutana, C. P. Collier, and K. P. Giapis, "Electrowetting in carbon nanotubes," *Science* **310**, 1480–1483 (2005).
18. N. R. Smith, L. Zhou, J. Zhang, and J. Heikenfeld, "Fabrication and demonstration of electrowetting liquid lens arrays," *J. Disp. Technol.* **5**, 411–413 (2009).
19. S. Berry, J. Kedzierski, and B. Abedian, "Low voltage electrowetting using thin fluoropolymer films," *J. Colloid Interface Sci.* **303**, 517 (2006).
20. A. A. Kornysheva, A. R. Kucernak, M. Marinescu, C. W. Monroe, A. E. S. Sleightholme, and M. Urbakh, "Ultra-low-voltage electrowetting," *J. Phys. Chem.* **114**, 14885 (2010).
21. S.-L. Lee and C.-F. Yang, "Numerical simulation for meniscus shape and optical performance of a MEMS-based liquid microlens," *Opt. Express* **16**, 19995–20007 (2008).
22. R. D. Niederriter, A. M. Watson, R. N. Zahreddine, C. J. Cogswell, R. H. Cormack, V. M. Bright, and J. T. Gopinath, "Individually addressable electrowetting lens arrays for adaptive optics," submitted to *Opt. Express*. (June 2012)
23. J. E. Kinsky, C. X. Yu, D. V. Murphy, S. E. J. Shaw, R. C. Lawrence, and C. Higgs, "Beam control of a 2D polarization maintaining fiber optic phased array with high-fiber count," *Proc. SPIE* **6306**, 63060G (2006).
24. R. J. Noll, "Zernike polynomials and atmospheric turbulence," *J. Opt. Soc. Am.* **66**, 207 (1976).